

Enhanced stability, bistability, and exceptional points in saturable active photonic couplersYertay Zhiyenbayev^{1,*}, Yannis Kominis^{2,†}, Constantinos Valagiannopoulos^{1,‡},
Vassilios Kovanis^{3,4} and Anastasios Bountis⁵¹*Department of Physics, Nazarbayev University, KZ-010000 Nur-Sultan, Kazakhstan*²*School of Applied Mathematical and Physical Science, National Technical University of Athens, GR-10682 Athens, Greece*³*Bradley Department of Electrical and Computer Engineering, Virginia Tech Research Center, Blacksburg, Virginia 22203, USA*⁴*CREOL, The College of Optics & Photonics, University of Central Florida, Orlando, Florida 32816, USA*⁵*Department of Mathematics, Nazarbayev University, KZ-010000 Nur-Sultan, Kazakhstan*

(Received 21 July 2019; published 23 October 2019)

A generic photonic coupler with active and lossy parts, gain saturation, and asymmetric characteristics is examined. Saturable activity is shown to be able to enhance the overall stability of the steady states, prevent evolution to undesirable unbounded modes, and allow for bistable operation in specific regions of the parametric space. Both stability and bistability are studied in the phase space of the system, where the basins of attraction of each state are identified, providing an accurate description of the dependence of the electric fields on the initial conditions. Continuous families of exceptional points are detected via suitable regulation of the coupling and asymmetry features of the configuration. In this way, a complete description of the nonlinear dynamics landscape is provided, which should be crucial for multiple application-driven designs incorporating such a ubiquitous optical component.

DOI: [10.1103/PhysRevA.100.043834](https://doi.org/10.1103/PhysRevA.100.043834)**I. INTRODUCTION**

The nonlinear coherent optical coupler [1,2] is one of the most fundamental elements for multiple key technological architectures and photonic integrated circuits [3], allowing for applications related to power-dependent directed transport of energy [4], unidirectional propagation [5], and optical isolation [6,7]. The possibility of engineering the gain and loss characteristics of such devices results in a rich set of non-Hermitian dynamical features that have no counterpart in conservative (Hermitian) configurations and has been analyzed for decades (see, e.g., [8,9]). The generality of the underlying model, consisting of coupled-mode equations, suggests its applicability to a wide class of isomorphic non-Hermitian dimers, describing other photonic devices such as twisted fiber amplifiers [10] as well as quantum systems [11,12].

Most of the setups considered so far are structurally symmetric, with balanced loss and gain leading to parity-time (PT) symmetric configurations; indeed, in recent years there has been tremendous progress in the theoretical formulations and experimental implementations of such systems [13–18]. The overall lossless nature of these layouts gives rise to optimal responses with large applicability potential spanning from single-mode lasing [19,20], coherent perfect absorption [21], and optical switches with plasmonic waveguides [14–17] to invisible acoustic sensors [18]. Furthermore, interesting features and properties like tunable quantum phase transitions [22] and whispering-gallery-mode resonances [23] were

revealed due to PT symmetry. Most importantly, the PT-symmetric condition, when imposed on nonlinear structures, has led to significant results related to active control of light [24], controlled power transport [25], and robust soliton propagation [26].

However, under the symmetric presence of activity and dissipation, the system often evolves to states with unbounded electric field amplitudes, which is undesirable for realistic applications. As an example, two waveguides [25] with identical wave propagation numbers and exactly opposite gain and loss coefficients support either an asymmetric unbounded state [27,28] or a symmetric bounded nonlinear supermode, therefore not allowing for capabilities of directed power transfer between the two waveguides in a stable fashion. A remedy to such an unwanted behavior is the introduction of gain/loss asymmetry, which, as has been recently shown, not only enhances the stability of the system [29], but also admits controlled directed power transport enabled by the emergence of additional strongly asymmetric modes [30]. It is worth mentioning that the asymmetry as a stabilizer has been considered for other non-Hermitian photonic systems consisting of coupled lasers [31,32] but also for more general configurations of paired oscillators [33]. In addition, investigations of the key role of asymmetry in the formation and propagation of self-localized beams in non-Hermitian setups have shown that continuous families of solitary waves can be formed under generic conditions, not necessarily restricted by symmetry requirements [34]; as a result, they exhibit a rich set of propagation features such as dynamical trapping and controllable routing once the gain and loss spatial distribution is properly engineered [35,36].

Apart from asymmetry in structure and excitation, another important characteristic determining the functionality

*yertay.zhiyenbayev@nu.edu.kz

†gkomin@central.ntua.gr

‡konstantinos.valagiannopoulos@nu.edu.kz

of paired optical components is saturation. This property expresses the difficulty of photonic matter to be receptive to fields of large magnitudes developed therein; accordingly, the texture of the material changes to prevent unbounded power increase within its volume. Such behavior also yields a nonlinear effect that is most commonly present in active media. Indeed, saturation exerts significant damping influence on the instability of evanescently coupled arrays [37], acting as a natural stability booster. Moreover, saturable active matter, except for being more realistic, has been utilized for the study of optical cavity effects in nanowire lasers and waveguides [38] and ultrafast all-optical absorption switches for photonic crystals [39].

In this work, we combine the aforementioned characteristics of asymmetry and saturation to study the dynamical features of continuous waves in a generic asymmetric active coupler with saturable gain. After analytically determining the fixed points corresponding to the nonlinear supermodes (NSs) of the system and characterizing their linear stability, we scan the parametric space and identify the response of the device. Due to the considered gain saturation, the stability of the system gets enhanced and under certain conditions bistability [40] emerges, which is the backbone of multiple memory [41] and filtering [42] applications. In cases where one or two stable NSs exist we examine the influence of the initial conditions on the response of the coupler and, by numerically computing the evolution of the excited fields, we provide reliable basins of attraction [43] for the stable NSs and the undesirable unbounded state that govern the operation of the setup. Such information is crucial when designing components for the dynamic reconfiguration between supported steady states [44] and high-precision measurement and detection [45]. Finally, we search the non-Hermitian structure of our system for spectral degeneracies known as exceptional points (EPs) [46] that are related to substantial sensitivity capabilities [47] as well as mode conversion utilities [48]. We believe that the thorough and multifaceted analysis of such a general layout, while mainly interesting for its nonlinear dynamics content, is most important for its usefulness to a wealth of applications that are involved.

II. COUPLED-MODE EQUATIONS AND NONLINEAR SUPERMODES

A. System model and coupled-mode equations

We consider a pair of parallel waveguides positioned along the z axis of our Cartesian coordinate system (x, y, z) , depicted in Fig. 1. $E_j(z)$ with $j = 1, 2$ are the electric field complex phasors in each waveguide j when dropping the transverse spatial dependence xy and the vectorial nature of the modes. The time dependence is of the form $\exp(-i\omega t)$ and propagation along the $z > 0$ axis is examined. The first waveguide ($j = 1$) is lossy and, in its linear operation, characterized by a complex propagation constant $(\beta_1 + i\alpha_1)$, while $\alpha_1 > 0$ measures the magnitude of the loss. The second waveguide ($j = 2$) has gain; thus, $\alpha_2 < 0$, and inevitably, its response is clipped by saturation with constant $\varepsilon > 0$. Both waveguides are nonlinear and obey the Kerr effect, namely, their refractive indexes are proportional to the squared field magnitude

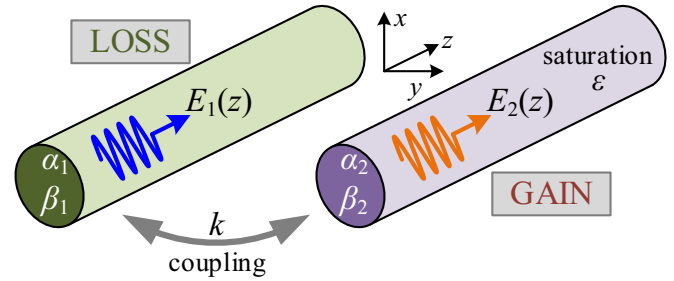


FIG. 1. Sketch of the examined setup. Two waveguides (one passive and one active) are evanescently coupled (by the constant k) and the developed waves $E_1(z)$ and $E_2(z)$ are propagating along axis z . The complex propagation constant of the passive waveguide is denoted $(\beta_1 + i\alpha_1)$ and that of the active waveguide (also saturable with saturation constant ε) $(\beta_2 + i\alpha_2)$.

with (common) proportionality constant γ . The two elements are evanescently coupled and their interaction is expressed through a positive linear coupling parameter $k > 0$ (nonlinear coupling is ignored).

Wave propagation into the aforementioned system is described by the following coupled-mode equations [49]:

$$-i \frac{dE_1}{dz} = (\beta_1 + i\alpha_1)E_1 + \gamma|E_1|^2E_1 + \frac{k}{2}E_2, \quad (1)$$

$$-i \frac{dE_2}{dz} = \left(\beta_2 + i \frac{\alpha_2}{1 + \varepsilon|E_2|^2} \right) E_2 + \gamma|E_2|^2E_2 + \frac{k}{2}E_1. \quad (2)$$

These coupled-mode equations are derived from the original Maxwell's laws, governing the wave propagation in a structure of evanescently coupled waveguides, under the paraxial approximation and by utilizing a perturbative approach. In particular, a single waveguide is considered as the unperturbed system and the presence of a second waveguide in its proximity acts as a perturbation. Each waveguide has its own set of eigenmodes that are orthogonal to each other; however, the perturbation destroys orthogonality and induces mode amplitude variation along the propagation distance. As a result, the energy exchange between the eigenmodes is described by the coupled-mode equations, through the coupling coefficient k given by the scaled overlap integral of the transverse eigenmodes of the two waveguides [50,51].

One may write the two complex fields in polar form, $E_j(z) = A_j(z) \exp[ibz + i\varphi_j(z)]$, with common propagation constant $b \in \mathbb{R}$, amplitudes $A_j > 0$, and phases $\varphi_j \in \mathbb{R}$, for $j = 1, 2$. If so, Eqs. (1) and (2) can be rewritten as follows by separating real from imaginary parts:

$$\dot{A}_1 = -\alpha_1 A_1 - \frac{k}{2} A_2 \sin \varphi, \quad (3)$$

$$\dot{A}_2 = -\frac{\alpha_2}{1 + \varepsilon A_2^2} A_2 + \frac{k}{2} A_1 \sin \varphi, \quad (4)$$

$$\dot{\varphi} = (\beta_2 - \beta_1) + \gamma(A_2^2 - A_1^2) + \frac{k}{2} \left(\frac{A_1}{A_2} - \frac{A_2}{A_1} \right) \cos \varphi, \quad (5)$$

where $\varphi = \varphi_2 - \varphi_1$ is the phase difference between the two waves and an overdot denotes the derivative with respect to z .

B. Nonlinear supermodes

The NSs of the system correspond to steady states propagating with constant values of the field amplitudes and phase difference $\{A_1, A_2, \varphi\}$. They can be found as fixed points of the dynamical system defined by Eqs. (3)–(5) by solving the nonlinear algebraic system obtained after setting the derivatives equal to 0. The NSs are completely described by four parameters, namely, the amplitude of one of the waveguides (A_1), the ratio of the squared field amplitudes [$R = (A_2/A_1)^2 > 0$], the phase difference (φ), and the propagation constant (b). The ratio R is found by solving the following fourth-order polynomial equation,

$$\left[\frac{\gamma}{\varepsilon}(\alpha R - 1) + \beta_1(\beta - 1) \frac{R}{R - 1} \right]^2 = \frac{k^2 R}{4} - \alpha_1^2, \quad (6)$$

where $\alpha = -\alpha_2/\alpha_1 > 0$ and $\beta = \beta_2/\beta_1 > 0$. These ratios of the imaginary and real parts of the refractive indices describe the asymmetry of the structure and are kept positive without loss of generality. Importantly, for $\alpha = \beta = 1$ and $\varepsilon = 0$, the system has a balanced gain and loss and the two waveguides have identical geometric properties determining their propagation constants, thus corresponding to a PT symmetric configuration [25]. The ratio R is restricted by the conditions

$$\left(\frac{k}{2\alpha_1} \right)^2 R > 1 \quad (7)$$

and

$$\gamma\beta_1(1 - R) \left(\beta - 1 \pm \frac{\alpha_1}{\beta_1} \frac{1 - R}{R} \sqrt{\left(\frac{k}{2\alpha_1} \right)^2 R - 1} \right) > 0, \quad (8)$$

reflecting the dependence of the asymmetry of the NSs on the parameters of the structure and defining the regions of parameter space where NSs exist. The other parameters characterizing the NSs are given in terms of R as follows:

$$\sin \varphi = -\frac{2\alpha_1}{k\sqrt{R}}, \quad (9)$$

$$A_1^2 = \frac{\alpha}{\varepsilon} - \frac{1}{\varepsilon R}, \quad (10)$$

and

$$b = \beta_1 \frac{\beta R - 1}{R - 1} + \frac{\gamma}{\varepsilon R} (\alpha R - 1)(R + 1). \quad (11)$$

In the absence of gain and loss saturation $\varepsilon \rightarrow 0$, the above expressions reduce to those obtained previously in [29,30]. It is worth emphasizing that there is a remarkable freedom in selecting the parameters of the system so that an asymmetric NS with arbitrary squared electric field amplitude ratio R exists, allowing for directed power transport capabilities.

The stability of the NS is determined by the eigenvalues of the Jacobian \mathbf{J} of the system evaluated at the specific NS,

$$\mathbf{J} = \begin{bmatrix} -\alpha_1 & -\frac{k}{2} \sin \varphi & -\frac{k}{2} A_2 \cos \varphi \\ \frac{k}{2} \sin \varphi & -\alpha_2 \frac{1 - \varepsilon A_2^2}{(1 + \varepsilon A_2^2)^2} & \frac{k}{2} A_1 \cos \varphi \\ \frac{(R+1)k \cos \varphi}{2A_2} - 2\gamma A_1 & 2\gamma A_2 - \frac{(R+1)k \cos \varphi}{2A_1 R} & \frac{(R-1)k \sin \varphi}{2\sqrt{R}} \end{bmatrix}, \quad (12)$$

with a positive real part of at least one eigenvalue corresponding to instability of the respective NS.

III. RESULTS AND DISCUSSION

A. Parameter-space analysis and stability maps

Prior to the presentation of results on the existence and stability of NSs, it would be meaningful to define value intervals for the quantities defining the structure and excitation of the investigated coupled system. In the following, we restrict our analysis to the case of $\gamma > 0$, corresponding to a self-focusing nonlinearity; the analysis is readily applicable to the case of self-defocusing nonlinearity $\gamma < 0$ due to the invariance of the system (1) and (2) under the “staggering” transformation $\gamma \rightarrow -\gamma$, $\beta_{1,2} \rightarrow -\beta_{1,2}$, $E_1 \rightarrow -E_1^*$, $E_2 \rightarrow E_2^*$. Moreover, γ is kept constant at $\gamma = 1$. This choice is based on the fact that A_1 and A_2 are normalized amplitudes usually possessing values of the order of unity; in this way, the nonlinear term becomes comparable in magnitude with the linear one, reinforcing the interplay between them. For similar reasons, we can use moderate values of the saturation parameter ε , in most cases within the interval $0 < \varepsilon < 1$, to avoid purging the gain factor. The coupling coefficient k , which is common to both waveguides due to reciprocity, is inversely proportional to the distance between the two waveguides since it is achieved via the evanescent waves developed outside of them; thus, we assume $k/|\beta_1| \in [0.1, 10]$. Finally, the ratios $\alpha, \beta > 0$, which indicate the asymmetry between the gain/loss distributions in the two waveguides and between the refractive indices of the two employed media, respectively, cover quite an extensive range: $0.1 < \alpha, \beta < 10$. Here, we care more about the effect of the asymmetry on the two coupled waveguides rather than the quantitative propagation features into each of them individually; therefore, we assume unitary values for the real and imaginary parts of the wavenumber ($\alpha_1 = \beta_1 = 1$) into the passive waveguide, without serious loss of generality.

The evolution of the system is crucially determined by the existence of stable NSs, and in fact, any realistic application is directly related to the existence of at least one stable NS. However, apart from converging to a stable NS, the system may evolve either to a trivial zero mode ($A_1 = A_2 = 0$) or to an unbounded state ($A_1 = 0, A_2 \rightarrow +\infty$) [25,30]. In the following, we sweep the basic parameters and we obtain detailed stability maps depicting the number of stable NSs in each region of parameter space. Regions with no stable NSs are indicated in blue, whereas regions with one or two stable NSs are designated by green and brown color, respectively.

In Fig. 2, we show the number of stable NSs supported by the system as a function of the gain/loss contrast α and propagation constant asymmetry β between the waveguides for various coupling and saturation levels. In Fig. 2(a), we examine a system with no saturation ($\varepsilon = 0$) and low coupling; it is noted that stability is achieved only within a moderate zone of α , while $\beta < 1$. Remarkably, the behavior of the coupled waveguides ceases to be stable abruptly for $\alpha > 1$, when the overall nature of the device becomes active. This is directly related to the symmetry of the dynamic equations (1) and (2) when $\varepsilon = 0$, which becomes perfect at the PT-symmetric point ($\alpha = \beta = 1$). One may wonder how it is possible to have

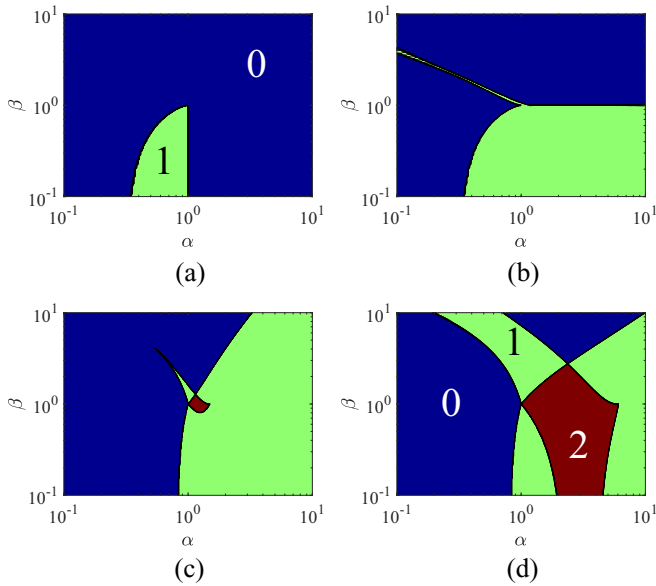


FIG. 2. Number of stable NSs (0, blue; 1, green; 2, brown) as a function of the gain/loss asymmetry α and propagation constant asymmetry β for (a) zero saturation $\varepsilon = 0$ and weak coupling, $k/\beta_1 = 2$; (b) $\varepsilon = 1$ and $k/\beta_1 = 2$; (c) $\varepsilon = 0.1$ and $k/\beta_1 = 10$; and (d) $\varepsilon = 1$ and $k/\beta_1 = 10$.

a stable mode for larger gain values α , whereas no such mode exists for very small gain values. Such a trend is attributed to the strong engagement of the active waveguide with the passive one, due to their coupling interaction; for a very weak coupling, the active part is left alone to continuously increase its mode amplitude even for small gain values.

In Fig. 2(b), we investigate the same setup as in Fig. 2(a) but with increased saturation ($\varepsilon = 1$). One directly observes the beneficial influence of saturation on the stability response. In particular, the system can be stable for more substantial gain ranges α ; indeed, increased saturation “clips” the activity of the gain medium and prevents A_2 from divergence. Note that in Fig. 2(b) an additional and ultranarrow stability region is opened for larger β , if properly matched with diminished gain/loss contrasts α . Importantly, the strong asymmetry between the two waveguides studied in Fig. 2 is exploitable in directed power transport [30] and control of modulational instability [29].

In Fig. 2(c), we increase the coupling, which enhances the collaboration towards stability of the two waveguides, compared with Figs. 2(a) and 2(b). In addition, it leads to the onset of bistability across a small parametric region close to the PT-symmetric regime. Such a conclusion is further validated by Fig. 2(d), where the same sizable coupling ($k/\beta_1 = 10$) is combined with significant saturation ($\varepsilon = 10$). A much more extended parametric “plateau” of bistability is formulated, accompanied by substantial restriction of unstable regions. Upon inspection of Figs. 2(c) and 2(d), we remark that bistability domains never share a common boundary with domains where no stable NSs exist; they only touch each other via isolated points. The bistability reported in Figs. 2(c) and 2(d), accompanied by hysteresis, is indispensable for information processing in various setups including acoustic

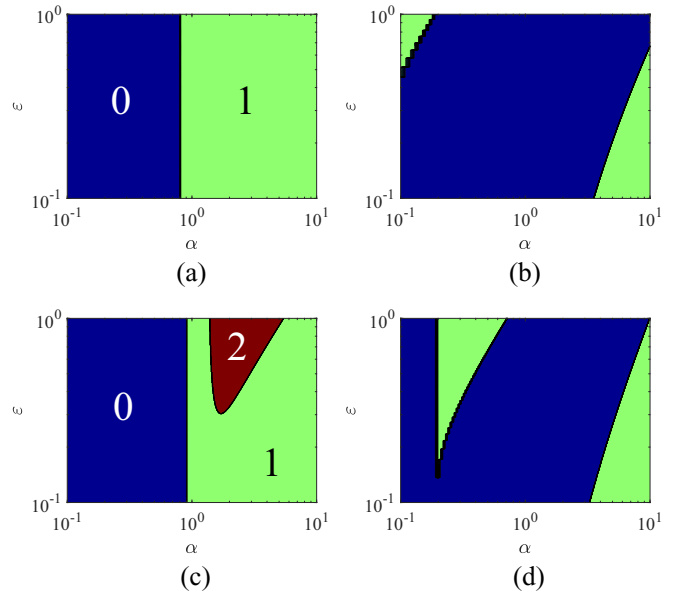


FIG. 3. Number of stable NSs (0, blue; 1, green; 2, brown) as a function of the gain/loss asymmetry α and saturation level ε for (a) a low propagation constant ratio, $\beta = 0.5$, and moderate coupling, $k/\beta_1 = 5$; (b) $\beta = 10$ and $k/\beta_1 = 5$; (c) $\beta = 0.5$ and $k/\beta_1 = 10$; and (d) $\beta = 10$ and $k/\beta_1 = 10$.

[52] or thermal [53] components and for photonic memory primarily in optical structures [41]. Similar bistability effects also occur in antidirectional couplers with gain and loss [54].

In Fig. 3 we display stability maps, as in Fig. 2, where we scan the whole range of the saturation coefficient ε . In Fig. 3(a), where low values of β and k are assumed, we observe an abrupt change in the stability behavior occurring at a specific value of $\alpha \cong 0.91$. In Fig. 3(b), we further increase β and note that stability is also achievable for low levels of α , unlike in Fig. 3(a); however, the system becomes overall more unstable [larger blue region compared to Fig. 3(a)]. In Fig. 3(c), where the coupling is stronger, bistability emerges for a considerable part of the stable parametric space, even though the unstable region remains almost unchanged. In Fig. 3(d) we examine the same pair of waveguides as in Fig. 3(b) but with a smaller distance between them (larger $k/\beta_1 = 10$); such a design modification allows the system to support a stable regime for very low saturation levels even when α is below unity. The stability features of saturable couplers enables their utilization as cells in a computing photonic platform [55] and for atom-photon coupling with high radiative decay [56].

In Fig. 4 we investigate how sweeping the range of k values affects the stability of the system and thus represents the number of stable NSs in maps whose vertical axis indicates the normalized variable k/β_1 (with $\beta_1 = 1$). In Fig. 4(a), we see that, for a small gain α , the existence of a stable NS is restricted to a thin parametric strip of the (α, k) map. However, if the gain/loss asymmetry α (for $\alpha_1 = 1$) exceeds a threshold, the coupling favors the convergence of solutions, and that is why large stability and bistability parametric domains emerge. In Fig. 4(b), where the range of saturation coefficient ε has been extended, we note the absence of stable

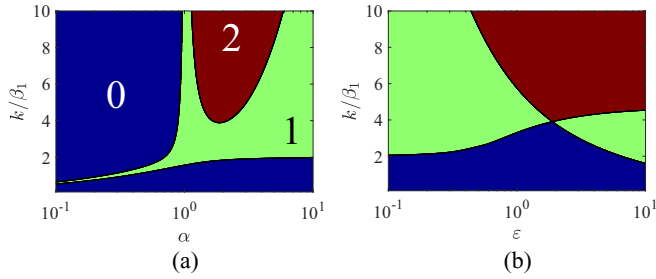


FIG. 4. Number of stable NSs (0, blue; 1, green; 2, brown) as a function of the normalized coupling k/β_1 and (a) the gain/loss asymmetry α (with $\beta = 0.8$, $\varepsilon = 1$) and (b) the saturation coefficient ε (with $\beta = 1.5$, $\alpha = 2$).

NSs for $k \rightarrow 0$. Furthermore, we again verify the findings shown in Figs. 2(c) and 2(d); indeed, the transition from two stable NSs to none occurs only through isolated points, unlike the transition from regions with two stable NSs to one or from one to none, which have common borders. Finally, Fig. 4(b) illustrates the crucial role of saturation in the bistability of the coupler; importantly, it seems that bistability is not feasible in the absence of saturation ($\varepsilon = 0$).

B. Phase-space analysis and basins of attraction

The existence of a stable NS does not guarantee the evolution of the system to this state; the system may evolve either to the stable zero state, an unbounded state, or one of the two stable NSs in the case of bistability, depending on the initial conditions $\{A_1(0), A_2(0), \varphi(0)\}$. By selecting the parameters of the system so that at least one stable NS exists we exclude the possibility of the system's evolution to the zero state, since it has been found to be stable only at parameter regions where no stable NS exists [30]. However, evolution to a specific stable NS (or the undesirable unbounded state) still depends strongly on the initial conditions. Each stable NS is associated with a basin of attraction, defined as the set of initial conditions for trajectories that asymptotically converge to this point. The extent of the basin of attraction of each stable NS in the system's phase space provides a measure of how "attractive" this NS is. In what follows, we show characteristic cases of basins of attraction calculated numerically by considering a fine grid of initial conditions on specific plane cuts of the three-dimensional phase space and characterize them according to their asymptotic evolution.

Such basins of attraction are sketched in Fig. 5(a) for the case of a single stable NS $\{\bar{A}_1, \bar{A}_2, \bar{\varphi}\}$ on an (A_1, A_2) map; the initial value $A_1(0)$ is represented along the horizontal axis and $A_2(0)$ along the vertical one. The third quantity, the phase difference, is kept fixed and equal to the steady-state value, namely, $\varphi(0) = \bar{\varphi}$. Green marks the basin of attraction of the stable NS, which is indicated by a black dot. Similarly, blue marks the basin of attraction of the unbounded state (instability region). It is noteworthy that apart from the main area containing the stable NS, the basin of attraction has a fine structure consisting of several thin strips, for larger $A_1(0)$, demonstrating the sensitive dependence on initial conditions, typical in complex nonlinear systems. To demonstrate the

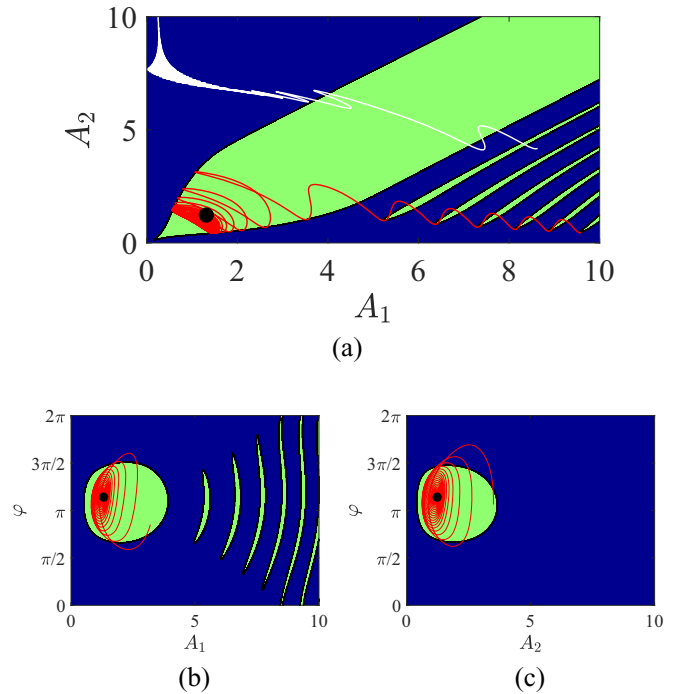


FIG. 5. Basins of attraction and representative solution trajectories on the initial condition planes. (a) $(A_1(0), A_2(0))$ map for $\varphi(0) = \bar{\varphi}$; (b) $(A_1(0), \varphi(0))$ map for $A_2(0) = \bar{A}_2$; (c) $(A_2(0), \varphi(0))$ map for $A_1(0) = \bar{A}_1$. The basin of attraction of the stable NS and the instability region are shown in green and blue, respectively. Plot parameters: $\alpha = 2$, $\beta = 1.5$, $\varepsilon = 0.5$, and $k/\beta_1 = 5$.

utility of the presented information, we show a couple of indicative trajectories of the system corresponding to initial conditions evolving asymptotically to the stable NS and the unbounded state. The red line corresponds to the solution trajectory beginning from one of the thin stable zones far away from the fixed point. We note that, after executing some oscillations and passing through instability domains [at which apparently $\varphi(z) \neq \bar{\varphi}$], the system converges to the steady-state solution. The case of initial conditions chosen within the blue region is illustrated by the white line in Fig. 5(a). Indeed, after some spatially abrupt changes, A_2 and A_1 tend monotonically to ∞ and 0 values, respectively.

In Fig. 5(b) we show the basins of attraction of the same system as in Fig. 5(a), but across a different plane cut with the phase difference $\varphi(0)$ at the vertical axis. It should be stressed that the two sketches [Figs. 5(a) and 5(b)] do not contain redundant information since this time the amplitude A_2 has been preselected equal to its convergent value, namely, $A_2(0) = \bar{A}_2$. We display a stable trajectory (red line) which, after following a spiral route, converges to the fixed point (black dot). In Fig. 5(c) we draw again the basins of attraction for the same configuration in the (A_2, φ) plane by choosing the initial amplitude $A_1(0)$ equal to \bar{A}_1 . We observe that in this plane cut the basin of attraction has a simply connected topology.

In Fig. 6, we investigate a coupled layout supporting two stable points, denoted by $\{\bar{A}_1, \bar{A}_2, \bar{\varphi}\}$ and $\{\hat{A}_1, \hat{A}_2, \hat{\varphi}\}$. Therefore, each triplet of initial conditions $\{A_1(0), A_2(0), \varphi(0)\}$ may give rise to a solution converging to one (green) or the other

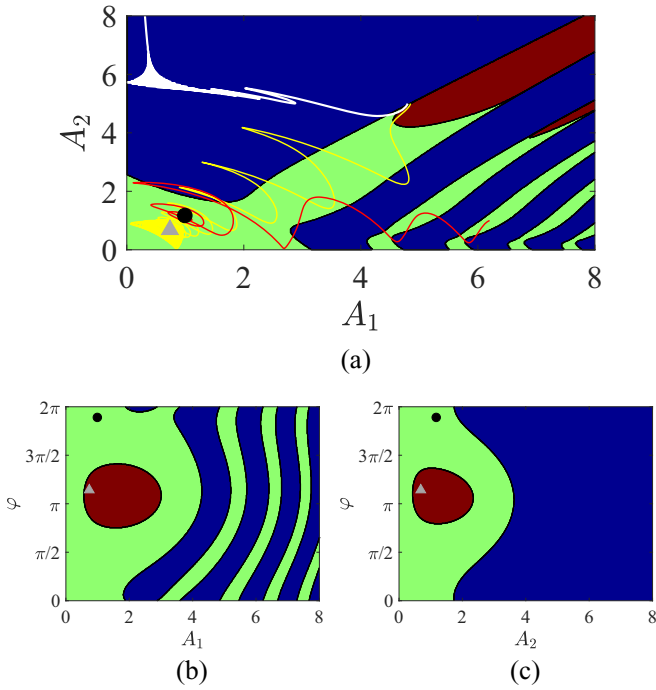


FIG. 6. Basins of attraction and representative solution trajectories in the initial condition planes of a system with two stable fixed points for (a) $\varphi(0) = \bar{\varphi}$, (b) $A_2(0) = \bar{A}_2$, and (c) $A_1(0) = \bar{A}_1$. The basins of attraction of the two stable NSs and the instability region are shown in green, brown, and blue, respectively. Plot parameters: $\alpha = 1.7$, $\beta = 1.4$, $\varepsilon = 1$, and $k/\beta_1 = 5$.

(brown) stable NS or may lead to instability. As implied above, the basins of attraction sketched on a two-dimensional plane cut require an implicit selection for the third parameter of our three-dimensional phase space, which has been taken equal to the corresponding value of the fixed point [like $\varphi(0) = \bar{\varphi}$ in Fig. 5(a)]. When bistability occurs, there are two alternatives for this selection (first or second stable NS), leading to different forms of basins of attraction shown in each plane cut.

In Fig. 6(a), we represent two fixed points, $\{\bar{A}_1, \bar{A}_2, \bar{\varphi}\}$ (black dot) and $\{\hat{A}_1, \hat{A}_2, \hat{\varphi}\}$ (gray triangle), on the (A_1, A_2) plane, implying that φ is respectively different; indeed, the two stable states are not so close to each other in the three-dimensional phase space as in Fig. 6(a), since $\bar{\varphi} \neq \hat{\varphi}$. However, the domains of stability and instability are computed considering that the initial phase difference φ is kept equal to that of the first NS: $\varphi(0) = \bar{\varphi}$. A major locus of stability is established, which is divided between the two stable NSs; it is again accompanied by thin strips similar to those in Fig. 5(a), but bicolored this time.

In Fig. 6(a) we also show characteristic evolutions of $A_1(z)$ and $A_2(z)$; one can observe a case converging to the first NS $\{\bar{A}_1, \bar{A}_2, \bar{\varphi}\}$ (red line), in a similar manner as in Fig. 5(a). In addition, we examine two neighboring initial points on the (A_1, A_2) plane exhibiting different behaviors for $z \rightarrow +\infty$ (one unstable, the other converging to the second NS). It is striking how they diverge from each other, with the first one (white line) following the path towards instability and the second (yellow line) spiraling around $\{\hat{A}_1, \hat{A}_2, \hat{\varphi}\}$.

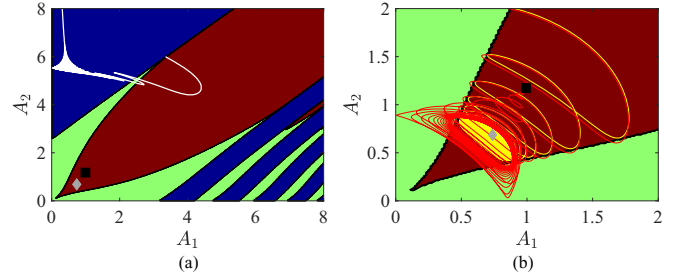


FIG. 7. Basins for attraction of the same system as in Fig. 6 but with the initial phase difference equal to the steady-state value of the other fixed point, $\varphi(0) = \hat{\varphi}$. (a) $(A_1(0), A_2(0))$ map; (b) detail of the $(A_1(0), A_2(0))$ map around the two fixed points. The basins of attraction of the two stable NSs and the instability region are shown in green, brown, and blue, respectively.

In Figs. 6(b) and 6(c), we calculate the basins of attraction with $A_2(0) = \bar{A}_2$ and $A_1(0) = \bar{A}_1$, respectively, as in Figs. 5(b) and 5(c). Obviously, the patterns are also 2π -periodic with respect to φ . Again, elongated segments of convergence to the first NS appear alternating with instability stripes. Furthermore, one can achieve convergence to $\{\bar{A}_1, \bar{A}_2, \bar{\varphi}\}$ even for $A_1(0) \rightarrow 0$, without caring much about $\varphi(0)$ as long as $A_2(0)$ is properly selected; on the contrary, one can reach $\{\hat{A}_1, \hat{A}_2, \hat{\varphi}\}$ only for a specific range of $\varphi(0)$, a result attributed to the choice $A_1(0) = \bar{A}_1$.

In Fig. 7 we sketch the basins of attraction for the same system as in Fig. 6 but with a different implicit selection of the third initial condition. In particular, in Fig. 7(a), we show the stability regions on the $(A_1(0), A_2(0))$ map with $\varphi(0) = \hat{\varphi}$; because of this alternative choice of $\varphi(0)$ compared to that in Fig. 6(a), the final states of the system are designated by the black square and gray rhombus. We emphasize that the shape of the domains is totally different, a feature which is again accredited to the three-dimensional nature of the problem making the two-dimensional cross cuts of convergence volumes for fixed $\varphi(0)$ [or one of the other two quantities $A_1(0)$ and $A_2(0)$] dependent on $\varphi(0)$ [or $A_1(0)$ and $A_2(0)$, respectively]. In particular, the extent of the basin of attraction corresponding to the first stable NS shrinks, whereas the other one dominates, in contrast to Fig. 6(a). Again, we show a characteristic trajectory for an initial condition chosen very close to but outside the basin of attraction of the stable NS; as in the corresponding trajectories in Figs. 5(a) and 6(a), the system evolves to the unbounded state with $A_1(z) \rightarrow 0$ and $A_2(z) \rightarrow +\infty$.

In Fig. 7(b), we show a detail of the bottom-left corner of the map in Fig. 7(a), together with two additional trajectories starting from two almost-adjacent initial points but belonging to different basins of attraction: one to the first NS (green region, red line) and the other to the second NS (brown region, yellow line). The projections of the two trajectories almost coincide initially; as z increases, the one starting from the basin of attraction of the second NS converges rapidly to the corresponding steady state with its amplitude undergoing multiple oscillations. However, the trajectory shown in red sticks on the second NS (gray rhombus), winding around it many times before finally reaching its own steady state (black

square). That feature of a solution spending a large part of its trajectory around the other steady state $\{\hat{A}_1, \hat{A}_2, \hat{\varphi}\}$ instead of its own $\{\hat{A}_1, \hat{A}_2, \hat{\varphi}\}$ seems definitely to be related with our initial phase difference choice, $\varphi(0) = \hat{\varphi}$. Such behavior of trajectories “sticking” at a point different from that of the final equilibrium is typical for complex nonlinear systems [43]. It is finally clear that small perturbations in initial conditions can cause the coupler response to move between the coexisting attractors, resulting in wild fluctuations in the power output [57].

C. Eigenvalue spectra and exceptional points

The eigenvalues λ of the Jacobian of the linearized system which determine its behavior around a mode of operation can coalesce for specific selections of parameters. Such a spectral degeneracy is typical for non-Hermitian systems (with gain and loss) and is known as an exceptional point; in its vicinity, the behavior of the system is of a fundamentally different nature compared to the neighboring points [58,59]. This spectral coincidence offers opportunities for ultrasensitive measurements [47,60] and other interesting applications involving energy transfer between developed waves [61,62]. Moreover, EPs have been shown to possess specific spectral signatures in the noise and modulation response [63] of non-Hermitian dimers and occur in abundance at the generic configuration of a dimer, not restricted by any symmetry conditions or other requirements related to the optical frequency mismatch and gain/loss ratio [64]. It is, therefore, meaningful to examine the occurrence of EPs in the system investigated in the present report. We have performed a thorough search across the considered parameter space in the quest for coalescing

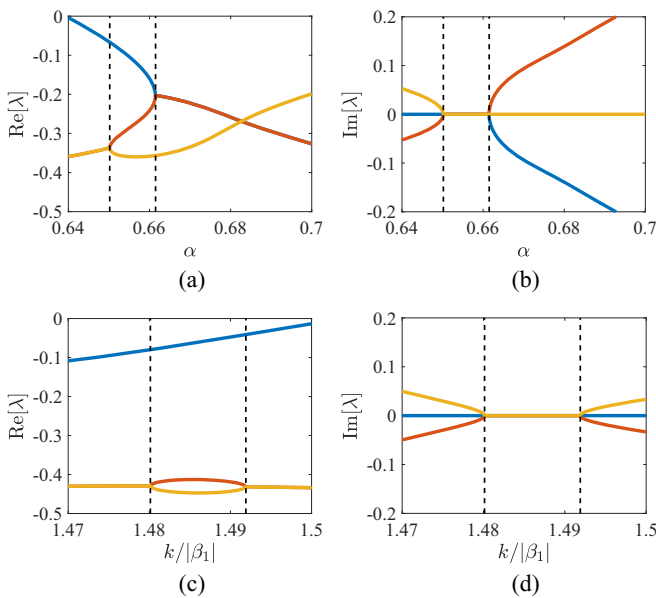


FIG. 8. (a) Real and (b) imaginary part of the eigenvalues as a function of the gain/loss contrast α for $k/|\beta_1| = 1.6$. (c) Real and (d) imaginary part of the eigenvalues as a function of the coupling $k/|\beta_1|$ for $\alpha = 0.565$. Dashed vertical lines denote exceptional points. Common plot parameters: $\beta = 1.012$, $\varepsilon = 0.8$, and $\beta_1 = -1$.

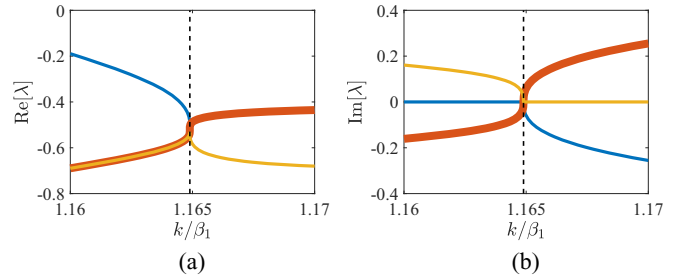


FIG. 9. (a) Real and (b) imaginary part of the eigenvalues as a function of the coupling k/β_1 for $\alpha = 0.521$. Dashed vertical lines denote EPs. Plot parameters: $\beta = 0.3$, $\varepsilon = 0.5$, and $\beta_1 = 1$.

eigenvalues λ and determined certain parametric loci along which such a degeneracy occurs in stable regions.

In Figs. 8(a) and 8(b), we show the variation of the real and imaginary parts of the three eigenvalues λ as a function of the gain/loss contrast α ; the black dashed vertical lines denote the emergence of EPs. Starting from Fig. 8(b), we observe that two EPs appear in pairs at those α 's that all three eigenvalues λ convert from complex into real, and vice versa; such a result is anticipated since the coefficients of the characteristic polynomial $|\mathbf{J} - \lambda\mathbf{I}|$ [with \mathbf{J} given by Eq. (12) and \mathbf{I} being the 3×3 identity matrix] are real. All these transitions happen within a restricted α range where the system is stable as indicated in Fig. 8(a) ($\text{Re}[\lambda] < 0$ for all eigenvalues). In Figs. 8(c) and 8(d), we show the dependence of the real and imaginary parts of λ 's, respectively, as functions of the coupling coefficient $k/|\beta_1|$. It seems that, by adjusting the distance between the two waveguides, one can achieve twice the coalescence of eigenvalues.

Finally, in Fig. 9, we show the case of an EP occurring at the coalescence of all three of the system's eigenvalues λ as the coupling k is swept for $\beta_1 > 0$. Two of the eigenvalues follow opposite trends in their real part and meet the third one at a specific k ; as far as the imaginary parts are concerned, they are vanishing only at the EP, unlike those in Figs. 8(b) and 8(d). We note again that a careful scanning of the coupling strength can lead to highly effective EP-based designs like polarization converters [65] and optical amplifiers [66].

IV. CONCLUDING REMARKS

The most generic configuration of an asymmetric active photonic coupler with saturable gain has been studied on the basis of coupled-mode equations valid for any non-Hermitian dimer. The saturation has been shown to result in significant stability enhancement of the nonlinear supermodes of the system, as well as avoidance of undesirable evolution to blowup solutions. The extent of the stability domains in parameter space, as well as the basins of attraction of the stable nonlinear supermodes in the phase space of the system, has been studied in detail. The critical role of asymmetry between the active and the passive waveguide parameters is demonstrated in terms of the number of supported nonlinear supermodes and the presence of bistability. Moreover, the existence of exceptional points in the linear spectrum of the stable modes has been shown to occur extensively in the parameter space of the system, namely, the spectral degeneracies are accessible

by varying any one of the key parameters. All these important features suggest that the asymmetric active photonic coupler is a fundamental element capable of reconfigurable functionality for photonic integrated circuit applications spanning from metrology and optical sensors to phase switching and ultrafast communications. Finally, we believe that the systematic investigation presented in this paper can be used to reveal the full complexity of the basins of attraction, not only of stable steady states, but also of other coexisting attractors, such as periodic oscillations (limit cycles); they are particularly relevant in optically injected photonic oscillators and systems of two optically coupled semiconductor lasers, where the

asymmetry and the nonlinear gain coefficient are seen to play a fundamental role.

ACKNOWLEDGMENTS

This work was supported by Nazarbayev University with Small Grant No. 090118FD5349 (“Super Transmitters, Radiators and Lenses via Photonic Synthetic Matter”) and ORAU Grant No. 2017-2020 on “Taming Chimeras to Achieve the Superradiant Emitter.” Funding from MES RK state-targeted program BR05236454 (Center of Excellence for Fundamental and Applied Physics, CEFAP) is also acknowledged.

-
- [1] S. M. Jensen, The nonlinear coherent coupler, *IEEE J. Quant. Electron.* **18**, 1580 (1982).
- [2] B. Daino, G. Gregori, and S. Wabnitz, Stability analysis of nonlinear coherent coupling, *J. Appl. Phys.* **58**, 4512 (1985).
- [3] B. E. A. Saleh and M. C. Teich, *Fundamentals of Photonics* (Wiley, New York, 2007).
- [4] L. Feng, Y.-L. Xu, W. S. Fegadolli, M.-H. Lu, J. E. B. Oliveira, V. R. Almeida, Y.-F. Chen, and A. Scherer, Experimental demonstration of a unidirectional reflectionless parity-time metamaterial at optical frequencies, *Nat. Mater.* **12**, 108 (2013).
- [5] L. Feng, M. Ayache, J. Huang, Y.-L. Xu, M.-H. Lu, Y.-F. Chen, Y. Fainman, and A. Scherer, Nonreciprocal light propagation in a silicon photonic circuit, *Science* **333**, 729 (2011).
- [6] D. Jalas *et al.*, What is—and what is not—an optical isolator, *Nat. Photon.* **7**, 579 (2013).
- [7] Y. Shi, Z. Yu, and S. Fan, Limitations of nonlinear optical isolators due to dynamic reciprocity, *Nat. Photon.* **9**, 388 (2015).
- [8] G. H. B. Thompson, Analysis of optical directional couplers that include gain or loss and their application to semiconductor slab dielectric guides, *J. Light. Technol.* **4**, 1678 (1986).
- [9] Y. Chen, A. W. Snyder, and D. N. Payne, Twin core nonlinear couplers with gain and loss, *IEEE J. Quant. Electron.* **28**, 239 (1992).
- [10] J. D. Huerta Morales, B. M. Rodriguez-Lara, and B. A. Malomed, Polarization dynamics in twisted fiber amplifiers: A non-Hermitian nonlinear dimer model, *Opt. Lett.* **42**, 4402 (2017).
- [11] V. M. Kenkre and D. K. Campbell, Self-trapping on a dimer: Time-dependent solutions of a discrete nonlinear Schrödinger equation, *Phys. Rev. B* **34**, 4959 (1986).
- [12] G. Dattoli, A. Torre, and R. Mignani, Non-Hermitian evolution of two-level quantum systems, *Phys. Rev. A* **42**, 1467 (1990).
- [13] R. El-Ganainy, M. Khajavikhan, D. N. Christodoulides, and S. K. Özdemir, The dawn of non-Hermitian optics, *Commun. Phys.* **2**, 37 (2019).
- [14] H. Alaeian and J. A. Dionne, Non-Hermitian nanophotonic and plasmonic waveguides, *Phys. Rev. B* **89**, 075136 (2014).
- [15] F. Monticone, C. A. Valagiannopoulos, and A. Alù, Parity-Time Symmetric Nonlocal Metasurfaces: All-Angle Negative Refraction and Volumetric Imaging, *Phys. Rev. X* **6**, 041018 (2016).
- [16] C. A. Valagiannopoulos, Optical PT-symmetric counterparts of ordinary metals, *IEEE J. Sel. Top. Quantum Electron.* **22**, 89 (2016).
- [17] A. Lupu, H. Benisty, and A. Degiron, Switching using PT symmetry in plasmonic systems: Positive role of the losses, *Opt. Express* **21**, 21651 (2013).
- [18] R. Fleury, D. Sounas, and A. Alù, An invisible acoustic sensor based on parity-time symmetry, *Nat. Commun.* **6**, 5905 (2015).
- [19] L. Feng, Z. J. Wong, R.-M. Ma, Y. Wang, and X. Zhang, Single-mode laser by parity-time symmetry breaking, *Science* **346**, 972 (2014).
- [20] H. Hodaei, M.-A. Miri, M. Heinrich, D. N. Christodoulides, and M. Khajavikhan, Parity-time-symmetric microring lasers, *Science* **346**, 975 (2014).
- [21] S. Longhi, PT-symmetric laser absorber, *Phys. Rev. A* **82**, 031801(R) (2010).
- [22] L. Feng, R. El-Ganainy, and L. Ge, Non-Hermitian photonics based on parity-time symmetry, *Nat. Photon.* **11**, 752 (2017).
- [23] B. Peng, S. K. Özdemir, F. Lei, F. Monifi, M. Gianfreda, G. L. Long, S. Fan, F. Nori, C. M. Bender, and L. Yang, Parity-time-symmetric whispering-gallery microcavities, *Nat. Phys.* **10**, 394 (2014).
- [24] S. V. Suchkov, A. A. Sukhorukov, J. Huang, S. V. Dmitriev, C. Lee, and Y. S. Kivshar, Nonlinear switching and solitons in PT-symmetric photonic systems, *Laser Photon. Rev.* **10**, 177 (2016).
- [25] H. Ramezani, T. Kottos, R. El-Ganainy, and D. N. Christodoulides, Unidirectional nonlinear PT-symmetric optical structures, *Phys. Rev. A* **82**, 043803 (2010).
- [26] V. V. Konotop, J. Yang, and D. A. Zezyulin, Nonlinear waves in PT-symmetric systems, *Rev. Mod. Phys.* **88**, 035002 (2016).
- [27] I. V. Barashenkov, G. S. Jackson, and S. Flach, Blow-up regimes in the PT-symmetric coupler and the actively coupled dimer, *Phys. Rev. A* **88**, 053817 (2013).
- [28] A. U. Hassan, H. Hodaei, M.-A. Miri, M. Khajavikhan, and D. N. Christodoulides, Integrable nonlinear parity-time-symmetric optical oscillator, *Phys. Rev. E* **93**, 042219 (2016).
- [29] Y. Kominis, T. Bountis, and S. Flach, Stability through asymmetry: Modulationally stable nonlinear supermodes of asymmetric non-Hermitian optical couplers, *Phys. Rev. A* **95**, 063832 (2017).
- [30] Y. Kominis, T. Bountis, and S. Flach, The asymmetric active coupler: Stable nonlinear supermodes and directed transport, *Sci. Rep.* **6**, 33699 (2016).
- [31] Y. Kominis, V. Kovanis, T. Bountis, Controllable asymmetric phase-locked states of the fundamental active photonic dimer, *Phys. Rev. A* **96**, 043836 (2017).

- [32] Z. Gao, S. T. M. Fryslie, B. J. Thompson, P. S. Carney, and K. D. Choquette, Parity-time symmetry in coherently coupled vertical cavity laser arrays, *Optica* **4**, 323 (2017).
- [33] J. D. Hart, Y. Zhang, R. Roy, and A. E. Motter, Topological Control of Synchronization Patterns: Trading Symmetry for Stability, *Phys. Rev. Lett.* **122**, 058301 (2019).
- [34] Y. Kominis, J. Cuevas-Maraver, P. G. Kevrekidis, D. J. Frantzeskakis, and A. Bountis, Continuous families of solitary waves in non-symmetric complex potentials: A Melnikov theory approach, *Chaos Solitons Fract.* **118**, 222 (2019).
- [35] Y. Kominis, Soliton dynamics in symmetric and non-symmetric complex potentials, *Opt. Commun.* **334**, 265 (2015).
- [36] Y. Kominis, Dynamic power balance for nonlinear waves in unbalanced gain and loss landscapes, *Phys. Rev. A* **92**, 063849 (2015).
- [37] D. T. Nichols and H. G. Winful, The effect of nonlinear gain on the stability of evanescently coupled semiconductor laser arrays, *J. Appl. Phys.* **73**, 459 (1993).
- [38] J. C. Johnson, H. Yan, P. Yang, and R. J. Saykally, Optical cavity effects in ZnO nanowire lasers and waveguides, *J. Phys. Chem. B* **107**, 8816 (2003).
- [39] H. Nakamura *et al.*, Ultra-fast photonic crystal/quantum dot all-optical switch for future photonic networks, *Opt. Express* **12**, 6606 (2004).
- [40] C. Thirstrup, Optical bistability in a nonlinear directional coupler, *IEEE J. Quant. Electron.* **31**, 2101 (1995).
- [41] Z. Huang, A. Baron, S. Larouche, C. Argyropoulos, and D. R. Smith, Optical bistability with film-coupled metasurfaces, *Opt. Lett.* **40**, 5638 (2015).
- [42] A. Rohm, K. Ludge, and I. Schneider, Bistability in two simple symmetrically coupled oscillators with symmetry-broken amplitude- and phase-locking, *Chaos* **28**, 063114 (2018).
- [43] J. M. T. Thompson and H. B. Stewart, *Nonlinear Dynamics and Chaos* (Wiley, New York, 2002).
- [44] I. Sliwa and K. Grygiel, Periodic orbits, basins of attraction and chaotic beats in two coupled Kerr oscillators, *Nonlin. Dynam.* **67**, 755 (2012).
- [45] I. Kozinsky, H. W. Ch. Postma, O. Kogan, A. Husain, and M. L. Roukes, Basins of Attraction of a Nonlinear Nanomechanical Resonator, *Phys. Rev. Lett.* **99**, 207201 (2007).
- [46] W. D. Heiss, The physics of exceptional points, *J. Phys. A* **45**, 444016 (2012).
- [47] H. Hodaie, A. U. Hassan, S. Wittek, H. Garcia-Gracia, R. El-Ganainy, D. N. Christodoulides, and M. Khajavikhan, Enhanced sensitivity at higher-order exceptional points, *Nature (London)* **548**, 187 (2017).
- [48] H. Wang, S. Assaworarith, and S. Fan, Dynamics for encircling an exceptional point in a nonlinear non-Hermitian system, *Opt. Lett.* **44**, 638 (2019).
- [49] W.-P. Huang, Coupled-mode theory for optical waveguides: An overview, *J. Opt. Soc. Am. A* **11**, 963 (1994).
- [50] G. P. Agrawal, *Applications of Nonlinear Fiber Optics* (Academic Press, New York, 2001), p. 63.
- [51] K. Okamoto, *Fundamentals of Optical Waveguides*, 2nd ed. (Academic Press, New York, 2006), p. 159.
- [52] O. R. Bilal, A. Foehr, and C. Daraio, Bistable metamaterial for switching and cascading elastic vibrations, *Proc. Natl. Acad. Sci. USA* **114**, 4603 (2017).
- [53] V. Kubytskyi, S.-A. Biehs, and P. Ben-Abdallah, Radiative Bistability and Thermal Memory, *Phys. Rev. Lett.* **113**, 074301 (2014).
- [54] A. Govindarajan, B. A. Malomed, and M. Lakshmanan, Non-linear anti-directional couplers with gain and loss, *Opt. Lett.* **44**, 4650 (2019).
- [55] C. Ríos, N. Youngblood, Z. Cheng, M. Le Gallo, W. H. P. Pernice, C. D. Wright, A. Sebastian, and H. Bhaskaran, In-memory computing on a photonic platform, *Sci. Adv.* **5**, eaau5759 (2019).
- [56] A. Goban, C.-L. Hung, S.-P. Yu, J. D. Hood, J. A. Muniz, J. H. Lee, M. J. Martin, A. C. McClung, K. S. Choi, D. E. Chang, O. Painter, and H. J. Kimble, Atom-light interactions in photonic crystals, *Nat. Commun.* **5**, 3808 (2014).
- [57] A. Prasad, Y.-C. Lai, A. Gavrielides, and V. Kovanis, Complicated basins in external-cavity semiconductor lasers, *Phys. Lett. A* **314**, 44 (2003).
- [58] M.-A. Miri and A. Alù, Exceptional points in optics and photonics, *Science* **363**, eaar7709 (2019).
- [59] S. Klaiman, U. Gunther, and N. Moiseyev, Visualization of Branch Points in PT-Symmetric Waveguides, *Phys. Rev. Lett.* **101**, 080402 (2008).
- [60] W. Chen, S. K. Ozdemir, G. Zhao, J. Wiersig, and L. Yang, Exceptional points enhance sensing in an optical microcavity, *Nature (London)* **548**, 192 (2017).
- [61] Y.-H. Lai, Y.-K. Lu, M.-G. Suh, and K. Vahala, Enhanced sensitivity operation of an optical gyroscope near an exceptional point, [arXiv:1901.08217](https://arxiv.org/abs/1901.08217).
- [62] S. N. Ghosh and Y. D. Chong, Exceptional points and asymmetric mode conversion in quasi-guided dual-mode optical waveguides, *Sci. Rep.* **6**, 19837 (2016).
- [63] Y. Kominis, V. Kovanis, and T. Bountis, Spectral signatures of exceptional points and bifurcations in the fundamental active photonic dimer, *Phys. Rev. A* **96**, 053837 (2017).
- [64] Y. Kominis, K. D. Choquette, T. Bountis, and V. Kovanis, Exceptional points in two dissimilar coupled diode lasers, *Appl. Phys. Lett.* **113**, 081103 (2018).
- [65] A. U. Hassan, B. Zhen, M. Soljacic, M. Khajavikhan, and D. N. Christodoulides, Dynamically Encircling Exceptional Points: Exact Evolution and Polarization State Conversion, *Phys. Rev. Lett.* **118**, 093002 (2017).
- [66] Q. Zhong, S. K. Ozdemir, A. Eisfeld, A. Metelmann, and R. El-Ganainy, Exceptional points-based optical amplifiers, [arXiv:1904.13005](https://arxiv.org/abs/1904.13005).